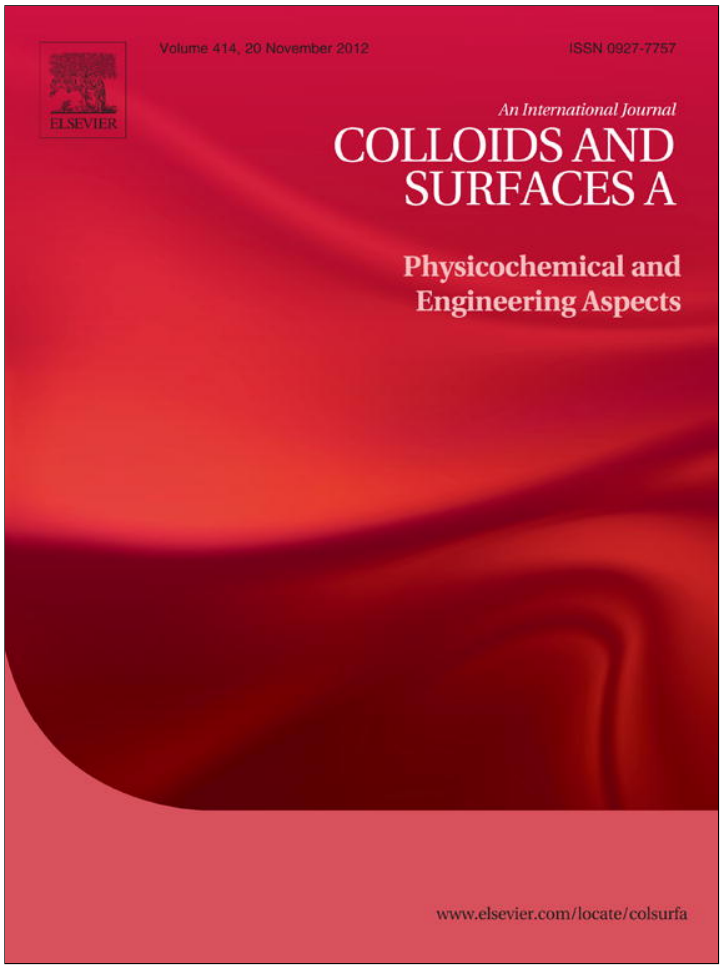

Colloids and Surfaces A: Physicochem. Eng. Aspects 414 (2012) 492–497

Contents lists available at SciVerse ScienceDirect

Colloids and Surfaces A: Physicochemical and Engineering Aspects

journal homepage: www.elsevier.com/locate/colsurfa

High-purity gold nanobipyramids can be obtained by an electrolyte-assisted and functionalization-free separation route

Zhirui Guo [a], Yu Wan [b], Meng Wang [b], Lina Xu [b], Xiang Lu [a,*], Guang Yang [b], Kun Fang [b], Ning Gu [b,**]

[a] The Second Affiliated Hospital of Nanjing Medical University, Nanjing 210011, China
[b] Jiangsu Key Laboratory for Biomaterials and Devices and State Key Laboratory of Bioelectronics, Southeast University, Nanjing 210096, China

HIGHLIGHTS

- Gold nanobipyramids with a purity of over 90% were firstly reported.
- The nano-mixtures subjected to shape-selective aggregation after adding salt.
- The aggregation of nanobipyramids was reversible and the reason was discussed.

GRAPHICAL ABSTRACT

.

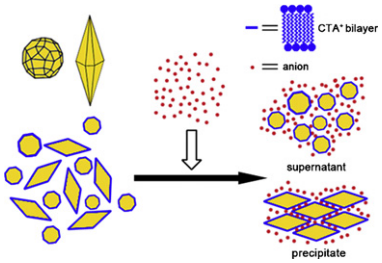

ARTICLE INFO

Article history:
Received 31 May 2012
Received in revised form 24 July 2012
Accepted 26 July 2012
Available online 10 August 2012

Keywords:
Gold nanobipyramid
Shape
Electrostatic screening
Contact area

ABSTRACT

Gold nanobipyramids (NBPs) have attracted intensive attentions because they exhibit more advantageous plasmonic properties than comparable gold nanorods. However, unlike that short gold nanorods can be synthesized routinely in a high yield (around 99% of the total particles), current syntheses of gold NBPs generally receive a low yield (around 30% of the total particles) and co-produce spherical impurities difficult to separate. Thus an effective purification route of gold NBPs is desirable for optimizing their performances. In this study, we demonstrated that the spherical nanoparticles with smaller inter-particle contact area can be separated from the NBPs that undergo gradual precipitation by electrolyte-induced electrostatic screening. During this procedure, no special surface-functionalization of the NBPs was needed. As a result of this simple separation strategy, NBPs at a level of purity to above 90% is achieved in a single purification round. In particularly, the precipitates of cetyltrimethylammonium bromide (CTAB)-capped NBPs can be easily converted into colloidal state due to the strong steric constraint of CTA^+ bilayer, facilitating further investigations.

1. Introduction

Control over the shape of noble metal nanocrystals has received growing interests because their plasmonic properties are highly shape-dependent [1–3]. Among numerous solution-based synthetic methods, preformed-seed-mediated growth has proven to be extremely powerful for the synthesis of a wide variety of multiply shaped nanocrystals with narrow size distribution [4,5]. For a case of seeding growth, shape-directing agent such as surfactant, polymer and foreign ion, is indispensable for breaking the symmetry of face-centered cubic noble metal to induce nonspherical structures [6–9]. On the other hand, the crystal type of the seeds is also important for shape evolution. An example can be given for the growth of elongated gold nanocrystals in the presence of cetyltrimethylammonium bromide (CTAB) and silver ions. When single-crystal seeds are used, the well-known short nanorods with a spectacular yield are obtained [10,11]. Interestingly, when the multiply-twinned seeds are exploited, bipyramid-shaped nanoparticles (NBPs) with twinned boundaries around the long axis are

* Corresponding author. Fax: +86 25 83575057.
** Corresponding author. Fax: +86 25 83272476.
E-mail addresses: luxiang1966@gmail.com (X. Lu), guning@seu.edu.cn (N. Gu).

0927-7757/$ – see front matter © 2012 Elsevier B.V. All rights reserved.
http://dx.doi.org/10.1016/j.colsurfa.2012.07.034

produced [12]. Theoretical calculations indicated that both the extinction cross-sections and local electric-field enhancements of gold NBPs are much larger than gold nanorods with comparable longitudinal surface plasmon resonance (LSPR) wavelengths [13,14]. Moreover, experimental studies revealed that gold NBPs own much higher refractive index sensitivity than short nanorods and spherical nanocrystals, which is beneficial to the improvement of LSPR-based immunoassay sensitivity [15–17]. In particularly, the LSPR properties of gold NBPs can also be tuned from visible to near infrared region by varying their aspect ratios (AR, defined as length/width), enabling them a promising candidate for photothermal therapy of cancer and in vivo surface-enhanced Raman spectroscopic detection [14,18]. While gold NBPs exhibit advantageous plasmonic properties, their low yield (around 30% of the total particles) by current synthetic methods remains a significant limitation for fully utilizing them. As an effort, Wang and co-workers [14] have modified the surfactants by using cetyltributylammonium bromide (CTBAB) instead to produce NBPs with a yield up to 50–60%. However, CTBAB is commercially unavailable and such a yield is still not ideal for practical applications. Very recently, Burgin et al. [19] revisited the crystal structure of gold NBPs using electron tomography. The 3D reconstruction reveals that NBPs have an irregular six-fold twinning structure with highly stepped facets, which is far from the generally described pentatwinned NBPs model formed from common pentatwinned seeds. This important observation indicates that the yield of gold NBPs is hard to be as high as that of gold nanorods due to the complex issue of the crystal nucleation and growth of gold NBPs. Therefore, purification of gold NPBs is necessary for optimizing their shape-dependent properties and expanding the applications. To date, most of studies on gold NBPs have to employ their mixtures and little attention has yet been devoted to achieve high-purity gold NBPs by a convenient post-preparative separation route.

In this work, we report that shape separation of gold NBPs from in-situ produced spherical impurities can be achieved by partially electrostatic screening through adding strong, nonreactive electrolyte such as NaCl. By doing this operation, NBPs subject to aggregation due to the relatively larger side contact area arising from their anisotropic shape, leaving most of the spherical ones in the supernatant. This simple while efficient strategy allows for the separated NBPs to above 90% purity after only a single purification round. Moreover, the as-separated CTA^+-capped NBPs show reversible aggregation due to the steric constraint by CTA^+ bilayer and thus can be easily converted into colloid by brief ultrasonication.

2. Materials and methods

2.1. Materials

CTAB was purchased from Sigma. Hydrogen tetrachloroaurate tetrahydrate ($HAuCl_4{\cdot}4H_2O$), silver nitrate ($AgNO_3$), sodium borohydride ($NaBH_4$), trisodium citrate dihydrate ($C_6H_5Na_3O_7{\cdot}2H_2O$), L-ascorbic acid ($C_6H_8O_6$), hydrochloric acid (HCl) and sodium chloride (NaCl) were all purchased from Shanghai Sinopharm Chemical Reagent Co. Ltd. (China). All the chemicals and reagents were used as received. Deionized water with resistance of 18 MΩ cm was used in all the experiments. All the glassware was cleaned by aqua regia ($HCl:HNO_3$ in a 3:1, v/v) and rinsed with deionized water prior to the experiments.

2.2. Synthesis of citrate-capped gold seeds

Tiny gold nanocrystals were synthesized as the seeds for the growth of gold NBPs by reducing $HAuCl_4$ with $NaBH_4$ in presence of trisodium citrate [20]. To a 40 mL solution containing 0.25 mM $HAuCl_4$ and 0.25 mM trisodium citrate under vigorous stirring, 1.0 mL of 100 mM freshly prepared $NaBH_4$ solution was added quickly at room temperature. The orange–red seed solution was aged at room temperature for at least 2 h before use in order to allow the complete hydrolysis of unreacted $NaBH_4$. UV–vis spectra showed that the characteristic plasmon resonance of the seed solution is at 500 nm (see Supporting information, Fig. S1), indicating that the sizes of as-produced gold nanocrytals were smaller than 10 nm.

2.3. Growth of gold NBPs

The crude gold NBPs solution grown from citrate-capped seeds was prepared by a one-step seed-mediated, silver ion and CTAB-assisted approach developed by Liu and Guyot-Sionnest [12]. Typically, a 100 mL of growth solution containing 0.5 mM $HAuCl_4$ and 0.1 M CTAB was prepared. To this solution was added 1 mL of 10 mM $AgNO_3$, 2 mL of 1.0 M HCl and 0.8 mL of 0.1 M L-ascorbic acid in turn and the resulting solution as growth solution was stirred gently. The orange color of the gold salt in the CTAB solution disappeared when L-ascorbic acid was added, due to the reduction of Au^{3+} to Au^+. The growth of gold NBPs was initiated by adding 0.8 mL of the seed solution to the growth solution. After the addition, the color of the growth solution changed from clear to violet red. The mixture solution was kept at 30 °C in water bath and left undisturbed overnight.

2.4. Procedure of shape separation

For a typical purification procedure of gold NBPs, the crude gold NBPs solution was firstly centrifuged at 11,000 g/min for 10 min to get rid of the extra CTAB. This treatment is necessary because that CTAB at a high concentration (0.1 M or more) is very easy to crystallize at room temperature. After centrifugation, the precipitates contained most of gold NBPs and byproducts were re-dispersed by the same volume of deionized water. The total concentration of the residual CTAB is ~5 mM. Next, a 20 mL of the NBPs dispersion was placed in a 50 mL plastic centrifuge tube followed the addition of 17.5 mL of 3.44 M NaCl aqueous solution and 2.5 mL deionized water. The mixture solution was then kept at ambient temperature without disturbance. After 24 h, the supernatant was taken and deionized water was added to the tube to disperse the precipitates. The precipitates were further converted into colloidal state by brief ultrasonication for optical characterization.

The effects of salt concentrations on the separation of NBPs were investigated as following: eight different sets of experiments were performed in eight 10 mL plastic centrifuge tubes. Each tube contained 4.0 mL of the NBPs dispersion and varying amounts (0.75, 1.0, 1.5, 2.5, 3.5, and 4.0 mL) of 3.44 M NaCl solution and (3.0, 3.5 and 4.0 mL) of 5.16 M NaCl solution. Proper amount of water was also added to these tubes for getting a total solution volume of 8.0 mL of each tube. Control experiment was conduced by mixing 4.0 mL of the NBPs dispersion with 4.0 mL water. These mixture solutions were kept at ambient temperature for 24 h without disturbance. After that, UV–vis spectra of the supernatant were recorded in a wavelength range of 300–900 nm using a quartz cuvette with 10 mm path length.

2.5. Characterization

Scanning electron microscopy (SEM) images were obtained by a Carl Zeiss ULTRA Plus Field Emission Scanning Electron Microscope with an accelerating voltage of 20.0 kV. The yields and average sizes of different gold nanocrystals were recorded by counting each nanocrystal in several SEM images and by measuring the sizes

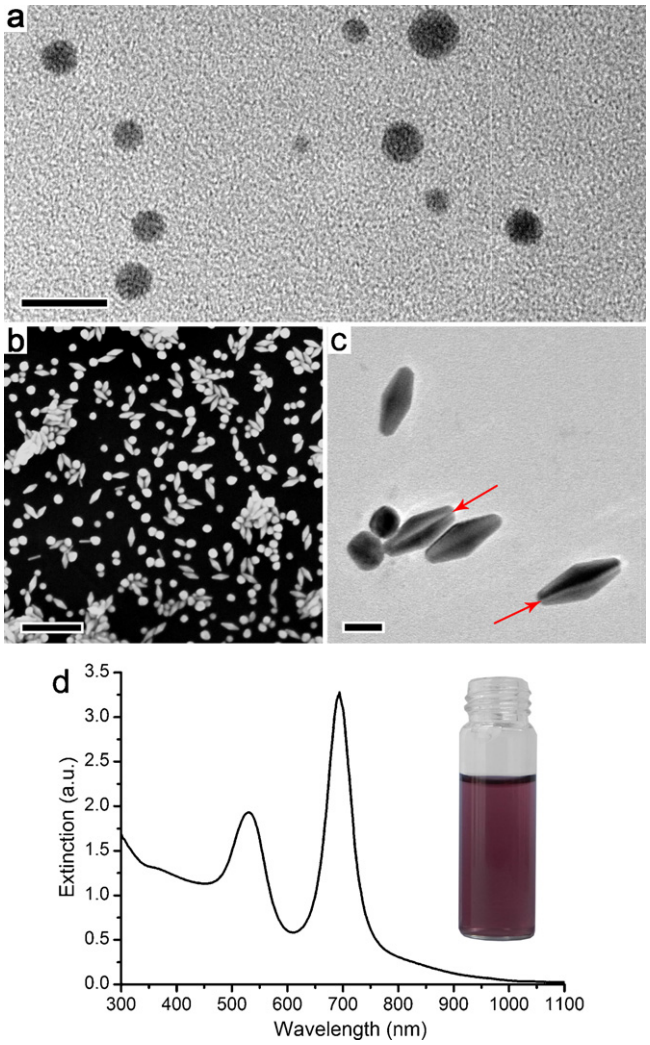

Fig. 1. (a) TEM image of the as-synthesized gold seeds, scale bar is 10 nm; (b) SEM and (c) TEM images of the gold products grown from the seeds, the twinned boundaries in the NBPs are labeled by arrows, scale bare is 200 nm in panel b and 20 nm in panel c, respectively; (d) UV–vis spectrum and photograph (inset) of the gold products.

using the Carl Zeiss software (Smart SEM). Transmission electron microscopy (TEM) images were taken with a JEM-2100EX (JEOL) transmission electron microscope operated at 200 kV. The UV–vis spectra were recorded by a Shimadzu UV-3600 spectrophotometer.

3. Results and discussion

Fig. 1a shows a TEM image of the citrate-capped gold seeds. It can be observed that these seeds are spherical in shape and have an average diameter of less than 5.0 nm. Fig. 1b present a typical SEM image of the as-obtained product grown form the above seeds. Three components are yielded, including faceted nanospheres (average 25 nm in diameter), monodisperse NBPs (average 50 nm in length and 21 nm in width) and a minute amount of nanorods (average 40 nm in length and 10 nm in width). While the previous report considered that citrate-capped seeds consist of multiply twinned nanocrytals, the generation of short nanorods strongly indicates that seeds also contain a few single crystals. The yield of NBPs was 39.6% and that of spherical ones was as high as 59.2% (Table S1). Corresponding TEM image of the product is shown in Fig. 1c. It can be seen that a clear twin boundary exists along the growth axis of a NBP, indicating that the NBPs are not in single-crystalline

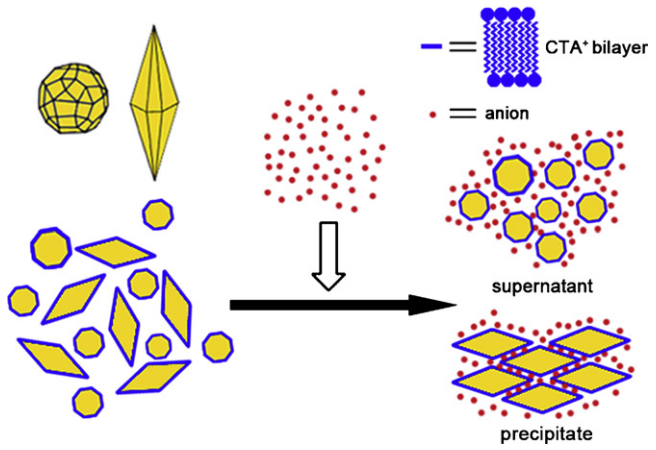

Fig. 2. Schematics of the shape-selective separation process induced by salt. The left upper inset shows the geometric models of a faceted nanosphere and a nanobipyramid.

nature. The colloidal solution of the NBPs mixture was violet–red, as shown in the inset of Fig. 1d. The corresponding UV–vis spectrum in Fig. 1d presents two SPR peaks (694 and 518 nm). Because the predicted LSPR wavelength of the presented nanorods using discrete dipole approximation (DDA) method (that is, $\lambda_{max} = 96AR + 418$, where $AR \approx 4.0$) is located at 802 nm, thus the strong and sharp peak at 694 nm could be ascribed to the LSPR of the NBPs. The short-wavelength peak at 530 nm primarily corresponds to the presence of a mass of spherical byproducts.

A simple calculation can reveal that the mass of a NBP with 50 nm length and 21 nm width is equivalent to that of a sphere with a diameter of 21 nm. Therefore, the above-produced NBPs and spherical ones (average 25 nm in diameter) are not suitable for either simple centrifugal separation or filter operation. In a recent study [21], we have observed that, under higher salt concentration, gold nanorods or nanoprisms can be separated from the isotropic nanocrystals due to their sharp shape-dependent colloidal stability. Hence, we believe that this purification strategy could also be applied in the present NBPs–nanoshperes system. According to classic DLVO theory, the stability of a colloidal particle is dependent upon its total potential energy function V_T, which is the sum of van der Waals attractive (V_A) and electrical double layer repulsive (V_R) forces that exist between particles as they approach each other due to the Brownian motion (Eq. (1)) [22].

$$V_T = V_A + V_R \tag{1}$$

$$V_A = \frac{A}{12\pi D^2} \tag{2}$$

$$V_R = 2\pi\varepsilon_O\varepsilon_R a\xi^2 \exp(-\kappa D) \tag{3}$$

where A is the Hamaker constant, D is the center-to-center distance of neighboring nanoparticles, a is the particle radius, ε_o is the dielectric constant of vacuum, ε_R is the relative dielectric constant of the solvent, κ is a function of the ionic composition and ξ is the zeta potential. As shown in Eqs. (2) and (3), the van der Waal attractive force is independent of the electrical state of the colloidal particles and thus the aggregation of gold nanocrystals is driven by decrease of the electrostatic repulsion. This could be achieved by increasing the ionic strength (i.e. electrolyte concentration) to decrease the zeta potential as well as the thickness of the electrical double layer. Based on above theoretical analysis, the present shape-selective separation process begins with the incubation of strong, neutral electrolyte NaCl solution with original colloidal products. Fig. 2 presents a schematic of the proposed mechanism for shape separation: the surfaces of CTA^+-capped (in an energetically favored bilayer form [23]) gold nanocrystals are partially bind by Cl^- ions,

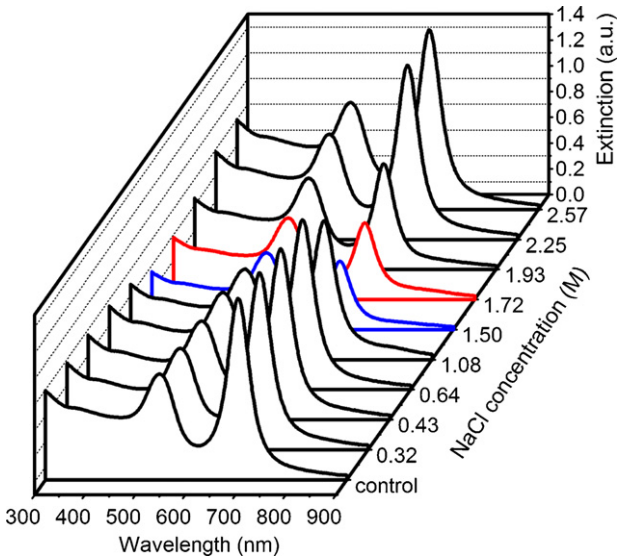

Fig. 3. UV–vis spectra of the supernatants of as-grown gold mixtures after the treatment with varied concentrations of NaCl for 24 h.

which breaks the balance between the electrostatic repulsion force and the short-range van der Walls attraction force and the distance between the nanocrystals is shorten. Therefore, the aggregation and precipitation of the nanocrystals would occur. Because the aqueous NBPs and spherical ones are both in a colloidal level, their gravitational force is insignificant as compared to Brownian motion. Thus the magnitude of the aggregation potential of the nanocrystals mainly depends on the maximal inter-particle contact area. Moreover, the produced nanocrystals with a certain shape commonly have a narrow size distribution in a case of seeding growth. That means each kind of nanocrystals owns a relatively constant contact area, facilitating the purification process. As a result, NBPs with a lager contact area at each side, rather than spherical nanocrystals with a larger mass, would go through aggregation and subsequent precipitation.

Fig. 3 summarizes UV–vis spectra from the supernatants of gold mixtures after treatment under varied NaCl concentrations for 24 h. In contrast with citrate-capped gold nanocrystals undergoing dramatic aggregation at a low NaCl concentration around 50 mM [24], these gold mixtures, either NBPs or spherical ones, hold excellent solution stability at concentrated NaCl concentrations due to the strong electrostatic repulsion forces offered by charge-rich CTA^+ bilayer. Furthermore, it is found that the NBPs exhibit an apparent solution stability threshold when the NaCl concentration is increased to 1.50 M (blue curve in Fig. 3). At this point, the peak intensity of NBPs (at LSPR wavelength) decreased dramatically while that of the spherical ones dropped slightly, indicating that a large amount of gold NBPs are separated from the solution. Note that the LSPR peak intensity decreases from 1.42 before salt treatment (control experiment) to 0.51 after salt treatment (at 1.50 M), indicating that 65% of NBPs were separated in a single purification round at the given incubation time. Furthermore, when the concentration of NaCl is increased to 1.72 M or more, the aggregative tendency of NBPs was not enhanced but reduced instead by judging from the increased LSPR peak intensity (red curve in Fig. 4). This phenomenon has been explained to arise from the neutralizing the surface charges and producing an electronic double layer on the gold surfaces by an excess number of anions [25]. Consequently, it should pay attention to the concentration of post-adding salt for avoiding the occurrence of disaggregation effect.

The as-obtained gold precipitates after NaCl treatment at a concentration of 1.50 M were observed by SEM. As shown in Fig. 4a and b, the precipitates consisted of uniform NBPs with purity above 90% and no nanorods were found (Table S2). It is worth noting that, in contrast with the reports that common citrate-capped gold nanocrystals undergo irreversible aggregation after NaCl treatment [24,26], these NBPs precipitates can be easily converted into colloid by brief ultrasonic treatment. As for the reason, it is believed that the ordered and dense CTA^+ bilayer on the longitudinal surface (side facets) of gold NBPs plays a key role. Very recently, Gomez-Grana et al. [27] reported the direct measure of the thickness of the CTA^+ bilayer on gold nanorods synthesized by the seeded growth

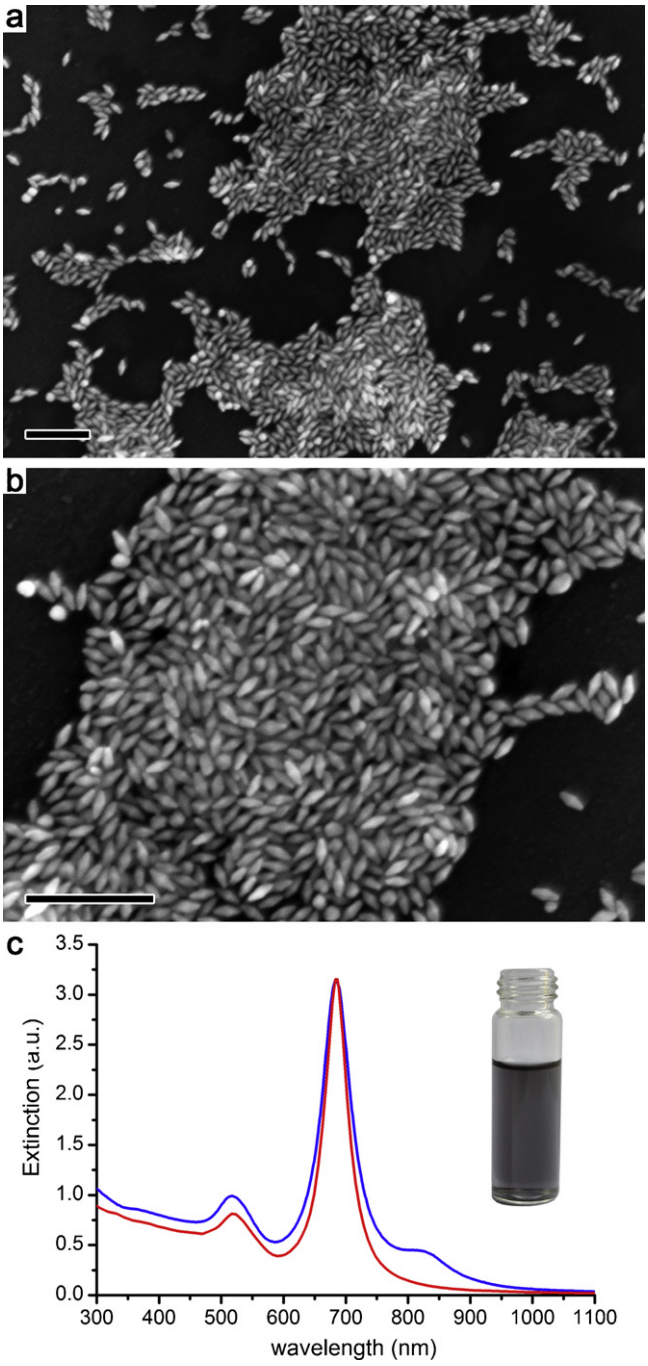

Fig. 4. SEM images of the as-separated gold NBPs at (a) low magnification and (b) high magnification, respectively. scale bar is 200 nm; (c) UV–vis spectrum of separated NBPs re-dispersion (blue curve) and DDA orientedly averaged calculated extinction spectrum for a NBP (red curve). The photograph (inset) shows the color of the solution of re-dispersed NBPs. (For interpretation of the references to color in this figure legend, the reader is referred to the web version of the article.)

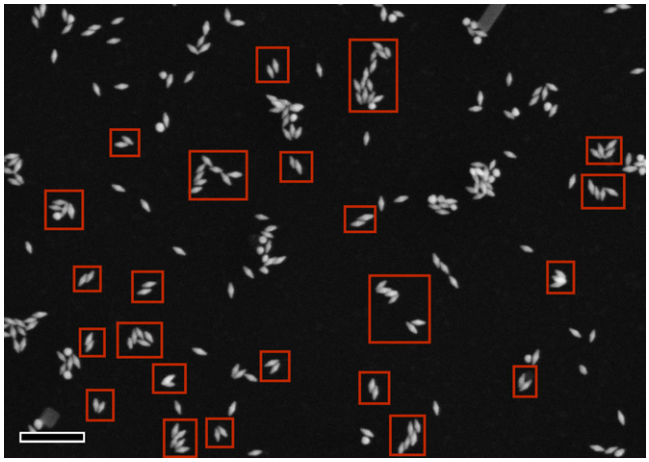

Fig. 5. Typical SEM image of the diluted gold NBPs. The as-formed NBPs oligomers are marked by red boxes, revealing that the NBPs prefer to contact in a side-by-side mode when approaching each other. Sale bar is 200 nm. (For interpretation of the references to color in this figure legend, the reader is referred to the web version of the article.)

method using small angle scattering of either X-rays or neutrons. Their work revealed that the thickness of a CTA^+ bilayer is about 3.2 nm, which is much higher of the citrate layer with a thickness of less than 0.5 nm [28]. Such thick surface coverage provides effective steric constraint to prevent the direct interaction between bare gold surfaces when the NBPs approach each other, enabling a reversible aggregation of the NBPs and avoiding the preformed surface functionalization. Therefore, when the desalting procedure is done by transferring the precipitated NBPs into deionized water, these NBPs can be converted into colloidal form by brief ultrasonication. Thanks for this result, the purity of the separated NBPs can thus allow for further examination by UV–vis spectroscopy. The short-wavelength peak of the re-dispersed NBPs decreased notably in intensity by comparison with that of the unpurified NBPs (see Fig. 1d) and had a 13 nm blue shift due to the removal of spheres (blue curve in Fig. 4c).

Correspondingly, the re-dispersed NBPs display a gray–blue color instead of the initial violet red. Note that the intensity ratio of longitudinal/short-wavelength peak significantly arises from 1.7 to 3.2 after purification, indicating a very high percentage of NBPs in the purified sample. Indeed, simulated spectrum obtained by DDA calculations is also in good agreement with the above measured spectrum (red curve in Fig. 4c and Fig. S2). Moreover, it is found a weak peak centered at 830 nm appears in the spectrum, which could be ascribed to the presence of a small amount aggregations of NBPs [29].

In a further study, we observed the naturally dried sample of the diluted gold NBPs by SEM in order to gain an insight into the aggregation mode of the NBPs. Fig. 5 presents a representative SEM image of the NPB oligomers. The observed results qualitatively revealed that NBPs, upon approaching each other, prefer to contact in a side-by-side mode but not an end-to-end fashion in order to reach a maximal contact area, consistent with the above-proposed mechanism.

4. Conclusion

In summary, we have demonstrated that the intrinsic shape discrepancy between NBPs and faceted spheres is the key element which allows for their separation through partially electrostatic screening by post-adding strong electrolyte. Importantly, the steric constraint by CTA^+ bilayer on the surfaces renders a reversible aggregation of these NBPs, facilitating down-stream investigations. Since CTAB as well as its homologues has become the most extensively applied capping agent in the syntheses of metal nanocrystals with numerous shapes, we envision that the separation method demonstrated here provides a simple avenue to purify a wide range of nanoscale mixtures toward their fundamental and practical applications.

Acknowledgments

We thank the Open Project by Jiangsu Key Laboratory of Biomaterials and Devices and the National Natural Science Foundation of China (Nos. 60725101, 30870679, 30970787) for the financial support.

Appendix A. Supplementary data

Supplementary data associated with this article can be found, in the online version, at http://dx.doi.org/10.1016/j.colsurfa.2012.07.034.

References

[1] S. Eustis, M.A. El-Sayed, Why gold nanoparticles are more precious than pretty gold: noble metal surface plasmon resonance and its enhancement of the radiative and nonradiative properties of nanocrystals of different shapes, Chem. Soc. Rev. 35 (2005) 209–217.
[2] L.M. Liz-Marzán, Tailoring surface plasmons through the morphology and assembly of metal nanoparticles, Langmuir 22 (2006) 32–41.
[3] T.K. Sau, A.L. Rogach, F. Jackel, T.A. Klar, J. Feldmann, Properties and applications of colloidal nonspherical noble metal nanoparticles, Adv. Mater. 22 (2010) 1805–1825.
[4] S.E. Skrabalak, Y. Xia, Pushing nanocrystal synthesis toward nanomanufacturing, ACS Nano 3 (2009) 10–15.
[5] T.K. Sau, A.L. Rogach, Nonspherical noble metal nanoparticles: colloid–chemical synthesis and morphology control, Adv. Mater. 22 (2010) 1781–1804.
[6] H.Y. Wu, H.C. Chu, T.J. Kuo, C.L. Kuo, M.H. Huang, Seed-mediated synthesis of high aspect ratio gold nanorods with nitric acid, Chem. Mater. 17 (2005) 6447–6451.
[7] W. Niu, S. Zheng, D. Wang, X. Liu, H. Li, S. Han, J. Chen, Z. Tang, G. Xu, Selective synthesis of single-crystalline rhombic dodecahedral, octahedral, and cubic gold nanocrystals, J. Am. Chem. Soc. 131 (2008) 697–703.
[8] Y. Xiong, I. Washio, J. Chen, H. Cai, Z.Y. Li, Y. Xia, Poly(vinyl pyrrolidone): a dual functional reductant and stabilizer for the facile synthesis of noble metal nanoplates in aqueous solutions, Langmuir 22 (2006) 8563–8570.
[9] T.H. Ha, H.-J. Koo, B.H. Chung, Shape-controlled syntheses of gold nanoprisms and nanorods influenced by specific adsorption of halide ions, J. Phys. Chem. C 111 (2007) 1123–1130.
[10] B. Nikoobakht, M.A. El-Sayed, Preparation and growth mechanism of gold nanorods (NRs) using seed-mediated growth method, Chem. Mater. 15 (2003) 1957–1962.
[11] T.K. Sau, C.J. Murphy, Seeded high yield synthesis of short Au nanorods in aqueous solution, Langmuir 20 (2004) 6414–6420.
[12] M. Liu, P. Guyot-Sionnest, Mechanism of silver (I)-assisted growth of gold nanorods and bipyramids, J. Phys. Chem. B 109 (2005) 22192–22200.
[13] M. Liu, P. Guyot-Sionnest, T.W. Lee, S.K. Gray, Optical properties of rodlike and bipyramidal gold nanoparticles from three-dimensional computations, Phys. Rev. B 76 (2007) 235428.
[14] X. Kou, W. Ni, C.K. Tsung, K. Chan, H.Q. Lin, G.D. Stucky, J. Wang, Growth of gold bipyramids with improved yield and their curvature-directed oxidation, Small 3 (2007) 2103–2113.
[15] H. Chen, X. Kou, Z. Yang, W. Ni, J. Wang, Shape- and size-dependent refractive index sensitivity of gold nanoparticles, Langmuir 24 (2008) 5233–5237.
[16] S. Lee, K.M. Mayer, J.H. Hafner, Improved localized surface plasmon resonance immunoassay with gold bipyramid substrates, Anal. Chem. 81 (2009) 4450–4455.
[17] J. Burgin, M. Liu, P. Guyot-Sionnest, Dielectric sensing with deposited gold bipyramids, J. Phys. Chem. C 112 (2008) 19279–19282.
[18] X. Kou, S. Zhang, C.K. Tsung, M.H. Yeung, Q. Shi, G.D. Stucky, L. Sun, J. Wang, C. Yan, Growth of gold nanorods and bipyramids using CTEAB surfactant, J. Phys. Chem. B 110 (2006) 16377–16383.
[19] J. Burgin, I. Florea, J. Majimel, A. Dobri, O. Ersen, M. Tréguer-Delapierre, 3D morphology of Au and Au@Ag nanobipyramids, Nanoscale 4 (2012) 1299–1303.
[20] J.E. Millstone, S. Park, K.L. Shuford, L. Qin, G.C. Schatz, C.A. Mirkin, Observation of a quadrupole plasmon mode for a colloidal solution of gold nanoprisms, J. Am. Chem. Soc. 127 (2005) 5312–5313.
[21] Z. Guo, X. Fan, L. Xu, X. Lu, C. Gu, Z. Bian, N. Gu, J. Zhang, Shape separation of colloidal gold nanoparticles through salt-triggered selective precipitation, Chem. Commun. 47 (2011) 4180–4182.

[22] D. Myers, Surfaces, Interfaces, and Colloids: Principles and Applications, 2nd ed., John Wiley & Sons, Inc., New York, 1999.
[23] C.J. Murphy, L.B. Thompson, A.M. Alkilany, P.N. Sisco, S.P. Boulos, S.T. Sivapalan, J.A. Yang, D.J. Chernak, J. Huang, The many faces of gold nanorods, J. Phys. Chem. Lett. 1 (2010) 2867–2875.
[24] T. Stakenborg, S. Peeters, G. Reekmans, W. Laureyn, H. Jans, G. Borghs, H. Imberechts, Increasing the stability of DNA-functionalized gold nanoparticles using mercaptoalkanes, J. Nanopart. Res. 10 (2008) 143–152.
[25] M. Sethi, G. Joung, M.R. Knecht, Stability and electrostatic assembly of Au nanorods for use in biological assays, Langmuir 25 (2009) 317–325.
[26] Z. Zhang, Y. Wu, Investigation of the $NaBH_4$-induced aggregation of Au nanoparticles, Langmuir 26 (2010) 9214–9223.
[27] S. Gomez-Grana, F. Hubert, F. Testard, A. Guerrero-Martinez, I. Grillo, L.M. Liz-Marzan, O. Spalla, Surfactant (bi)layers on gold nanorods, Langmuir 28 (2012) 1453–1459.
[28] Z. Lee, K.J. Jeon, A. Dato, R. Erni, T.J. Richardson, M. Frenklach, V. Radmilovic, Direct imaging of soft–hard interfaces enabled by graphene, Nano Lett. 9 (2009) 3365–3369.
[29] P.K. Jain, S. Eustis, M.A. El-Sayed, Plasmon coupling in nanorod assemblies: optical absorption, discrete dipole approximation simulation, and exciton-coupling model, J. Phys. Chem. B 110 (2006) 18243–18253.